

## 2D evaluation of crack openings using smeared and embedded crack models

André Luís Gamino\*<sup>1</sup>, Osvaldo Luís Manzoli<sup>2</sup>,  
José Luiz Antunes de Oliveira e Sousa<sup>1</sup> and Túlio Nogueira Bittencourt<sup>3</sup>

<sup>1</sup>University of Campinas, 13083-852, Campinas, Brazil

<sup>2</sup>UNESP - Univ Estadual Paulista, 17030-360, Bauru, Brazil

<sup>3</sup>University of São Paulo, 05508-900, São Paulo, Brazil

(Received September 18, 2009, Accepted June 23, 2010)

**Abstract.** This work deals with the determination of crack openings in 2D reinforced concrete structures using the Finite Element Method with a smeared rotating crack model or an embedded crack model. In the smeared crack model, the strong discontinuity associated with the crack is spread throughout the finite element. As is well known, the continuity of the displacement field assumed for these models is incompatible with the actual discontinuity. However, this type of model has been used extensively due to the relative computational simplicity it provides by treating cracks in a continuum framework, as well as the reportedly good predictions of reinforced concrete members' structural behavior. On the other hand, by enriching the displacement field within each finite element crossed by the crack path, the embedded crack model is able to describe the effects of actual discontinuities (cracks). This paper presents a comparative study of the abilities of these 2D models in predicting the mechanical behavior of reinforced concrete structures. Structural responses are compared with experimental results from the literature, including crack patterns, crack openings and rebar stresses predicted by both models.

**Keywords:** finite elements, fracture mechanics, smeared crack model, embedded crack model.

---

### 1. Introduction

The pioneering work by Prof. Scordelis in the 1960s (Bresler and Scordelis 1963) plays an important role in the evolution of nonlinear finite element analysis of reinforced concrete structures, defining concepts and criteria followed by the community of researchers in this area. Based on the numerous contributions of Prof. Scordelis, classic laboratory tests performed on twelve reinforced concrete beams to investigate shear behavior have been used to support numerical development in this subject.

A simple model developed by Ngo and Scordelis (1967) contributed significantly to the numerical simulation of cracking in concrete structures. In their paper, Ngo and Scordelis (1967) presented a simple numerical method to evaluate the bond-slip effect between rebars and the surrounding concrete using bond links.

Since then, these results have been widely used as a benchmark for calibration and validation of numerical modeling of reinforced concrete structures. Recently, Vecchio and Shim (2004) conducted another experimental program based on the same Bresler-Scordelis beams, in which the post-peak

---

\* Corresponding author, Ph.D., E-mail: [andre.gamino@gmail.com](mailto:andre.gamino@gmail.com)

behavior was monitored in terms of load-displacement curves. The authors observed that the behavior of the tested beams is strongly influenced by crushing of concrete. They also found that in the case of the beams without stirrups, failure is influenced by the bottom reinforcements at the plate end.

In former papers (Lorrain *et al.* 2007, Gamino *et al.* 2007 and Gamino *et al.* 2009), the authors presented simulations of Bresler-Scordelis beams (1967) using smeared crack models, embedded rebars and concrete-rebar debonding effects using commercial and in-house software. Further details of these implementations are found in Gamino (2007), Gamino and Bittencourt (2007), and Jacomassi *et al.* (2009).

More recently, embedded crack finite elements became an important tool to describe strong discontinuity formation and propagation in initially continuous media (Jirásek 2000 made a comprehensive review of the first works). This technique allows for the crack effects to be included in standard underlying finite elements during the loading process, independently of the position of the crack surface with respect to the finite element boundaries.

Embedded crack finite elements have only very recently been applied by Oliver *et al.* (2008) and Manzoli *et al.* (2008) to describe the behavior of reinforced concrete members, after the development of numerical techniques that increased the stability and robustness of this approach to deal with multiple cracks.

This paper presents the first comparative study of some aspects of the mechanical behavior of reinforced concrete beams predicted by the two aforementioned approaches: rotational smeared crack and embedded crack elements.

## 2. Embedded crack finite element

The formulation proposed by Manzoli and Shing (2006) is chosen for the embedded representation of cracks inside finite elements. This formulation is based on an enrichment of the finite element strain field to account for the effects of a crack line formation in its interior, with arbitrary position of the element's boundaries. This approach provides a consistent way to describe crack formation and propagation using a fixed finite element mesh, defined prior to the analysis of the original (continuous) concrete.

The crack formation zone is modeled by introducing a very thin interface band into the finite element, whose behavior is described by a continuum damage constitutive model, in the context of the Continuum Strong Discontinuity Approach (CSDA) proposed by Oliver and coworkers (Oliver *et al.* 1999, Oliver 2000, Oliver *et al.* 2008, Manzoli and Shing 2006 and Manzoli *et al.* 2008). The damage criterion is based on the concrete tension strength,  $f_t$ , and the softening law provides energy dissipation compatible with the concrete fracture energy,  $G_f$ .

Although dealing with a continuum constitutive (stress-strain) relation at the interface, it can be shown that this is equivalent to an approach using a discrete (cohesive) constitutive relation, involving displacement jumps and stresses (Oliver 2000).

The embedded crack element was applied recently by Oliver *et al.* (2008) and Manzoli *et al.* (2008) to model reinforced concrete members, treating the rebars and the surrounding concrete as an equivalent composite material composed of steel fibers embedded in a homogeneous matrix (concrete) according to the mixture theory. A global algorithm was used to track multiple crack paths that usually occur in reinforced concrete members.

This paper uses a simpler approach. The concrete is modeled by solid elements and the

reinforcement bars are modeled by truss finite elements connected to the nodes of the solid finite elements. Therefore, the crack formation in concrete is described by the same approach used for homogeneous material, but with the ability to represent multiple crack paths. For this purpose, instead of a global tracking algorithm, a local tracking algorithm is used (described in section 2.3) to build paths from any finite element where a crack may initiate during the loading process.

### 2.1 Finite element formulation

Consider the three-node finite element with domain  $\Omega_e$  (Fig. 1), crossed by a discontinuity interface,  $S_{e2}$  which splits the finite element into two parts, isolating node 1 from the others. Let  $\mathbf{n} = \{n_x, n_y\}^T$  be the unit vector normal to the interface and  $\mathbf{m} = \{m_x, m_y\}^T$  the unit vector normal to the element's side opposite the isolated node (see Fig. 1(a)). The discontinuity of the displacement field (strong discontinuity) at the interface produces a relative rigid-body motion between the two parts of the element, leading to the following nodal displacements (see Fig. 1(c))

$$\mathbf{d}_1 = [[\mathbf{u}]]; \mathbf{d}_2 = \mathbf{0}; \mathbf{d}_3 = \mathbf{0} \quad (1)$$

where  $\mathbf{d}_i (i=1,2,3)$  is the displacement vector of node  $i$ , produced by the displacement jump at the interface, whose components are encompassed in the vector  $[[\mathbf{u}]]$ . The strains of the element's continuous parts,  $\boldsymbol{\varepsilon} = \{\varepsilon_x, \varepsilon_y, \gamma_{xy}\}^T$ , can be obtained by the standard strain-displacement relation of the underlying finite element, so that

$$\boldsymbol{\varepsilon} = \sum_{i=1}^3 \mathbf{B}_i (\mathbf{D}_i - \mathbf{d}_i) = \sum_{i=1}^3 \mathbf{B}_i \mathbf{D}_i - \mathbf{B}_1 [[\mathbf{u}]] = \mathbf{B} \mathbf{D} - \boldsymbol{\varepsilon}^{cr} \quad (2)$$

where  $\mathbf{D}_i$  and  $\mathbf{B}_i$  represent, respectively, the total displacement vector and the standard finite element strain-displacement matrix of node  $i$ , and  $\boldsymbol{\varepsilon}^{cr} = \mathbf{B}_1 [[\mathbf{u}]]$  is the part of the strain field associated to the rigid-body motion due to the discontinuity, which can be written as

$$\begin{Bmatrix} \varepsilon_x^{cr} \\ \varepsilon_y^{cr} \\ \gamma_{xy}^{cr} \end{Bmatrix} = \frac{1}{l_e} \underbrace{\begin{bmatrix} m_x & 0 \\ 0 & m_y \\ m_y & m_x \end{bmatrix}}_{\mathbf{M}} \begin{Bmatrix} [[u]]_x \\ [[u]]_y \end{Bmatrix} = \frac{\mathbf{M}}{l_e} [[\mathbf{u}]] \quad (3)$$

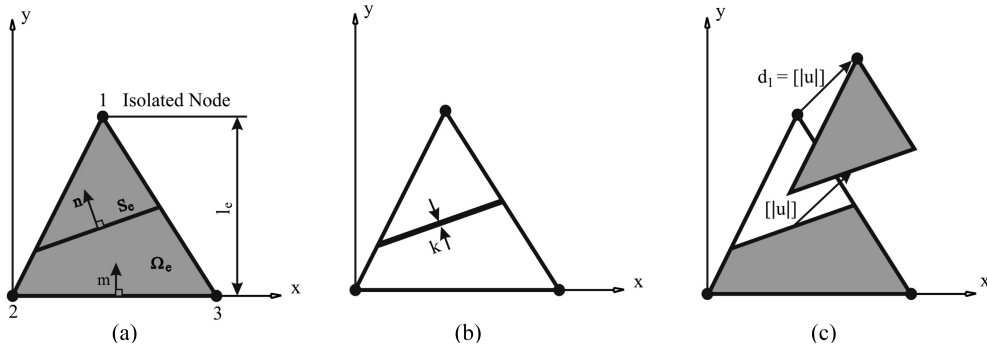


Fig. 1 Embedded crack finite element

where  $\mathbf{M}$  is the matrix casting the components of the vector  $\mathbf{m}$  and  $l_e$  is the distance between the isolated node and its opposite side (see Fig. 1(a)).

Assuming elastic behavior in the continuous part of the element, the corresponding stresses,  $\boldsymbol{\sigma} = \{\sigma_x, \sigma_y, \tau_{xy}\}^T$ , are given by

$$\boldsymbol{\sigma} = \mathbf{C}\boldsymbol{\varepsilon} = \mathbf{C}\left(\mathbf{B}\mathbf{D} - \frac{\mathbf{M}}{l_e}[[\mathbf{u}]]\right) \quad (4)$$

where  $\mathbf{C}$  is the constitutive elastic matrix. Therefore, the contribution of the internal force vector of a finite element with area  $A_e$  is given by

$$\mathbf{f}_{int} = \int_{\Omega_e} \mathbf{B}^T \boldsymbol{\sigma} d\Omega_e = \mathbf{B}^T \boldsymbol{\sigma} A_e = \mathbf{B}^T \mathbf{C} \left( \mathbf{B}\mathbf{D} - \frac{\mathbf{M}}{l_e} [[\mathbf{u}]] \right) A_e \quad (5)$$

From the CSDA (Oliver *et al.* 1999), the strains and corresponding stresses in the interface can be written as

$$\boldsymbol{\varepsilon}_S = \boldsymbol{\varepsilon} + \frac{\mathbf{N}}{k} [[\mathbf{u}]] = \mathbf{B}\mathbf{D} - \frac{\mathbf{M}}{l_e} [[\mathbf{u}]] + \frac{\mathbf{N}}{k} [[\mathbf{u}]] \quad (6)$$

$$\boldsymbol{\sigma}_S = \boldsymbol{\Sigma}(\boldsymbol{\varepsilon}_S) \quad (7)$$

where  $k$  is the width of the assumed thin localization band, whose mean line is the interface line (see Fig. 1(b)).  $\boldsymbol{\Sigma}(\boldsymbol{\varepsilon}_S)$  represents the continuum constitutive model for the interface, which returns the stress state to a given strain state and its history, and

$$\mathbf{N}^T = \begin{bmatrix} n_x & 0 & n_y \\ 0 & n_y & n_x \end{bmatrix} \quad (8)$$

The formulation is completed by the local traction continuity equation for each element, which enforces continuity between the bulk stresses,  $\boldsymbol{\sigma}$ , and discontinuity interface stresses,  $\boldsymbol{\sigma}_S$

$$\mathbf{N}^T(\boldsymbol{\sigma}_S - \boldsymbol{\sigma}) = 0 \quad (9)$$

which, after substituting the expressions (6), (7) and (4), reads

$$\mathbf{N}^T \sum \left( \mathbf{B}\mathbf{D} - \frac{\mathbf{M}}{l_e} [[\mathbf{u}]] + \frac{\mathbf{N}}{k} [[\mathbf{u}]] \right) - \mathbf{N}^T \mathbf{C} \left( \mathbf{B}\mathbf{D} - \frac{\mathbf{M}}{l_e} [[\mathbf{u}]] \right) = \mathbf{0} \quad (10)$$

In the framework of a displacement-based incremental and iterative procedure, for a given nodal displacement vector,  $\mathbf{D}_i^d$ , related to the iteration  $i$  of the load increment  $n$ , it is possible to solve the nonlinear Eq. (10) for the displacement jump,  $[[\mathbf{u}]]_i^n$ . The corresponding internal force vector can then be evaluated by Eq. (5). The element's tangent stiffness matrix associated to this procedure is given by

$$\mathbf{K} = \frac{\partial \mathbf{f}_{int}}{\partial \mathbf{D}} = \left\{ \mathbf{B}^T \mathbf{C} \mathbf{B} - \mathbf{B}^T \mathbf{C} \frac{\mathbf{M}}{l_e} \left[ \mathbf{N}^T \bar{\mathbf{C}} \left( \frac{\mathbf{M}}{l_e} - \frac{\mathbf{N}}{k} \right) - \mathbf{N}^T \mathbf{C} \frac{\mathbf{M}}{l_e} \right]^{-1} \mathbf{N}^T (\bar{\mathbf{C}} - \mathbf{C}) \mathbf{B} \right\} A_e \quad (11)$$

where  $\bar{\mathbf{C}} = \partial \boldsymbol{\Sigma} / \partial \boldsymbol{\varepsilon}_S$  is the interface tangent constitutive matrix.

### 2.2 Damage constitutive model

The damage constitutive model for the interface, denoted previously by  $\Sigma(\epsilon)$ , is defined by the following set of equations

$$\sigma = (1-d)\bar{\sigma}; \bar{\sigma} = \mathbf{C}:\epsilon \quad (\text{constitutive relation}) \quad (12)$$

$$f(\epsilon, r) = \tau_\epsilon - r \leq 0; \tau_\epsilon = \sqrt{\bar{\sigma}^+ : (\mathbf{C})^{-1} : \bar{\sigma}^+} \quad (\text{damage criterion}) \quad (13)$$

$$r(t) = \max_{s \in [0, t]} [r_0, \tau_\epsilon(s)]; r_0 = \frac{f_t}{\sqrt{E}} \quad (\text{evolution of the strain-like internal variable}) \quad (14)$$

$$d = 1 - \frac{r_0}{r} e^{\left(1 - \frac{r_0}{r}\right) \frac{r_0^2}{G_f}} \quad (\text{damage evolution with exponential softening law}) \quad (15)$$

where  $\bar{\sigma}$  is the effective stress tensor,  $\mathbf{C}$  is the elastic constitutive tensor,  $d$  is the damage variable,  $r$  is the strain and stress-like internal variable,  $f_t$  is the tensile strength,  $E$  is Young's modulus, and  $\bar{\sigma}^+$  is the positive part of the effective stress tensor, which contains only the positive principal stresses of  $\bar{\sigma}$ .

### 2.3 Crack tracking scheme

For the 2D analysis described in this paper, each crack path was constructed during the loading process by introducing straight lines into the elements, oriented according to the maximum principal stress when the stress state reaches the damage criterion, forming a continuous polygonal line, as shown in Fig. 2. Crack paths were allowed to start from several elements situated at the boundaries of the beams, chosen prior to the analysis (see Fig. 9). The crack formation and evolution from these elements depend on the stress state during the loading process.

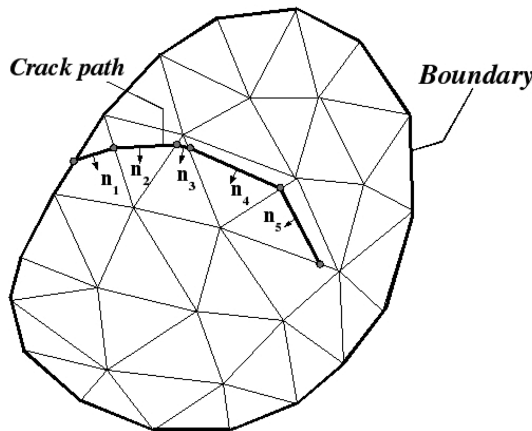


Fig. 2 Crack tracking scheme

### 3. Smearred crack model

The implementation of a rotational smeared crack model follows the strategy defined by Jirásek and Zimmermann (1998). This strategy defines the determination of the strain vector using the following expressions

$$\boldsymbol{\varepsilon} = \boldsymbol{\varepsilon}_e + \boldsymbol{\varepsilon}_{cr} \tag{16}$$

$$\boldsymbol{\sigma} = \mathbf{C} \boldsymbol{\varepsilon}_e \tag{17}$$

$$\underbrace{\begin{Bmatrix} \varepsilon_x \\ \varepsilon_y \\ \gamma_{xy} \end{Bmatrix}}_{\boldsymbol{\varepsilon}} = \frac{\boldsymbol{\sigma}}{E} \underbrace{\begin{Bmatrix} 1 \\ -\nu \\ 0 \end{Bmatrix}}_{\boldsymbol{\varepsilon}_e} + \frac{w_{cr}}{2A} \underbrace{\begin{Bmatrix} y_1 - y_2 \\ 0 \\ x_2 - x_1 \end{Bmatrix}}_{\boldsymbol{\varepsilon}_{cr}} \tag{18}$$

where  $\boldsymbol{\varepsilon}_e$  is the elastic strain vector,  $\boldsymbol{\varepsilon}_{cr}$  is the cracking strain vector,  $\boldsymbol{\varepsilon}$  is the total strain vector,  $A$  is the area of the finite element,  $w_{cr}$  is the crack width,  $\nu$  is Poisson's ratio, and  $x_i$  and  $y_i$  are the nodal coordinates.

Vector  $\boldsymbol{\varepsilon}_e$  corresponds to the elastic strains obtained from the Young modulus and Poisson ratio adopted here, and  $\boldsymbol{\varepsilon}_{cr}$  are the strains resulting from the material degradation process.

Crack openings also depend on the assumed softening model and are dependent on the stress level in the region of tension. The reinforcement rates affect the stress level on the tension side of the structure and, consequently, affect the crack openings (higher reinforcement rates imply smaller crack openings). As a consequence, crack openings are smaller at higher reinforcement ratios.

The following linear softening model is adopted, according to Fig. 3 and Eq. (19).

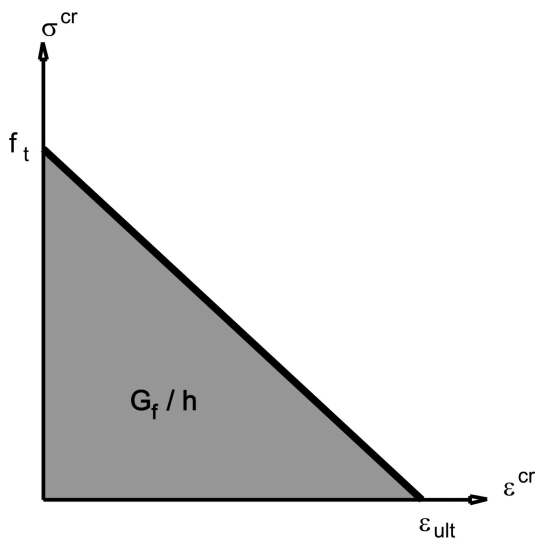


Fig. 3 Linear softening model

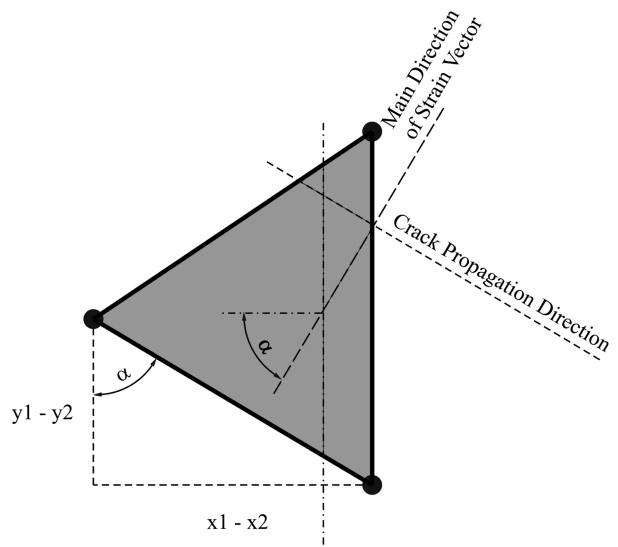


Fig. 4 Direction of crack propagation

$$\sigma(w_{cr}) = \begin{cases} f_t - f_t \frac{w_{cr}}{w_{cr,max}} \rightarrow 0 < w_{cr} < w_{cr,max} \\ 0 \rightarrow w_{cr,max} < w_{cr} < \infty \end{cases} \quad (19)$$

Finally, a definition of the crack propagation direction is necessary. This can be done by using the strain vector components  $\varepsilon$  (see Eq. (20) and Fig. 4). The angle  $\alpha$  indicates the principal strain direction and, orthogonal to this axis, the direction of propagation can be computed from

$$\alpha = \frac{1}{2} \arctan \frac{\gamma_{xy}}{\varepsilon_x - \varepsilon_y} \quad (20)$$

#### 4. Computational modeling

Based on the above formulations for the embedded or smeared crack representations, computational

Table 1. Mechanical properties of the concrete used for beam modeling

Property	Bresler and Scordelis (1963): Smeared crack	Bresler and Scordelis (1963): Embedded crack	Vecchio and Shim (2004): Smeared crack	Vecchio and Shim (2004): Embedded crack
$E$ [MPa]	30,000	30,000	34,300	34,300
$n$	0.15	0.15	0.15	0.15
$A$	1.80	---	1.93	---
$B$	3.25	---	3.27	---
$f_c$ [MPa]	37.6	37.6	43.5	43.5
$K_1$	11.59	---	11.56	---
$K_2$	0.98	---	0.99	---
$b$	0.2	---	0.2	---
$f_t$ [MPa]	4.14	4.14	3.13	3.13
$G_f$ [N/mm]	0.100	0.100	0.100	0.100
Crack band width [mm]	5.0	5.0	1.0	1.0

Table 2. Mechanical properties of the reinforcing bars used for beam modeling

Property	Bresler and Scordelis (1963)	Vecchio and Shim (2004)
$E$ [MPa]	218,000	210,000
$\nu$	0.30	0.30
$f_y$ [MPa]:		
Top reinforcement	---	315
Bottom reinforcement	555	445
Stirrup	---	600
$A_s$ :		
Top reinforcement	---	3 $\phi$ 11.3 mm
Bottom reinforcement	6 $\phi$ 28.7 mm	3 $\phi$ 29.9 mm and 2 $\phi$ 25.2 mm
Stirrup	---	$\phi$ 3.7 mm at 152 mm
Constitutive model	von Mises	von Mises

modeling was performed on reinforced concrete beams tested in Berkeley by Bresler and Scordelis (1963), and in Toronto by Vecchio and Shim (2004).

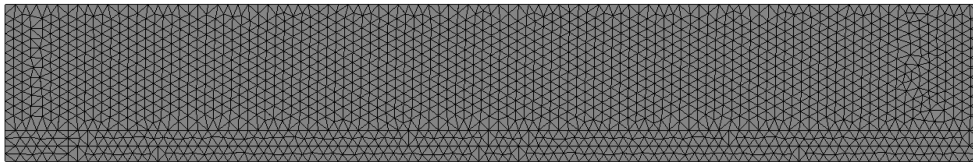
The reinforcement steel is modeled by truss finite elements connected to the nodes of the solid finite elements, so that perfect adherence between concrete and rebars is assumed. The nonlinear behavior of the steel bars is described by a one-dimensional elastic-perfectly plastic constitutive model.

Table 1 and Table 2 present the mechanical properties of the concrete and steel assumed for the beam modeling, based on the ones reported for the experimental tests. The typical meshes used in the FE simulations for the tested beams are depicted in Fig. 5.

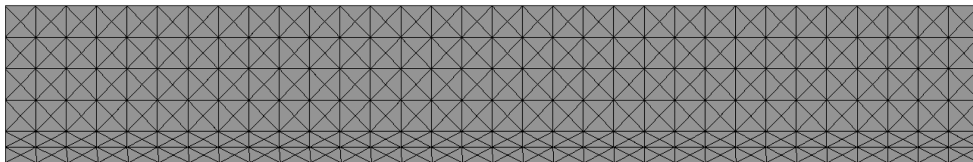
Since the embedded crack formulation presented here can describe only one crack per element, the corresponding mesh must be fine enough to properly capture the expected multiple cracks, with small spacing typically induced by the presence of reinforcement.

On the other hand, the smeared crack model deals with the crack at the integration point level and it is therefore able to describe the effects of cracks with small spacing using larger elements, with the expense of using higher-order elements.

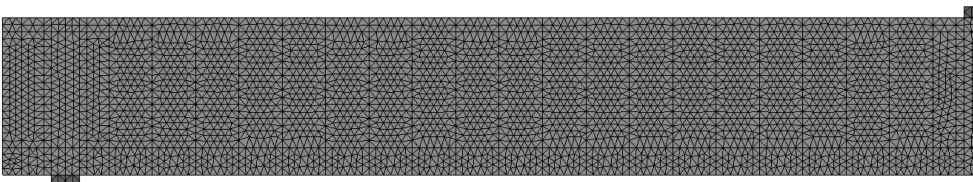
The meshes used for the analyses with the embedded crack model are constituted of three-node



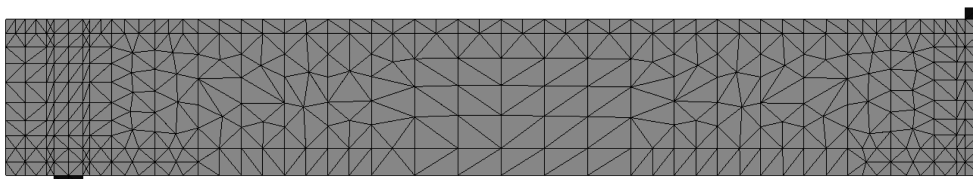
(a) Scordelis's beam with embedded cracks: 3,708 finite elements



(b) Scordelis's beam with smeared cracks: 768 finite elements



(c) Vecchio's beam with embedded cracks: 6,798 finite elements



(d) Vecchio's beam with smeared cracks: 718 finite elements

Fig. 5 Typical meshes used in nonlinear FE simulations

triangular (constant strain) elements. The meshes for the analyses with the smeared crack model, albeit coarser than those of the embedded crack formulation, consist of six-node triangular elements with quadratic interpolation functions.

The crack pattern in the smeared crack model can be illustrated in the post-process images by straight lines located at the integration points and oriented according to the direction of the crack (see Figs. 9(a) and 13(a)). The crack opening for each integration point is the internal variable  $w_{cr}$  of the cohesive constitutive model of Eq. (19). This variable can be displayed in post-process images, as indicated in Figs. 10(a) and 14(a).

In the embedded crack model, the crack pattern can be observed by plotting the polygonal lines constructed by the tracking algorithm (section 2.3) during the loading process (see Figs. 9(b) and 13(b)). In this model, the crack opening for each element can be obtained by projecting the displacement jump  $[[\mathbf{u}]]$  in the direction normal to the crack line (see Figs. 10(b) and 11(b)).

#### 4.1 Scordelis's beam

The OA3 beam, one of the classic rectangular beams tested in Berkeley, was modeled by using the smeared and embedded crack representations. Fig. 6 illustrates details of the test setup and beam geometry.

Numerical responses resulting from the modeling were compared to experimental results by Bresler and Scordelis (1963) in terms of force-displacement curves (Fig. 7) and force-strain in the

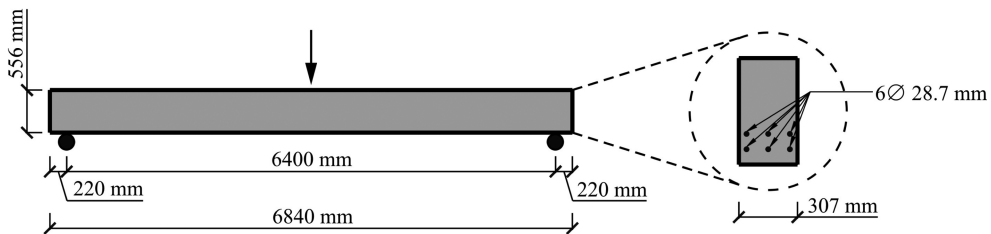


Fig. 6 Test setup for the OA3 beam tested in Berkeley (Bresler and Scordelis 1963)

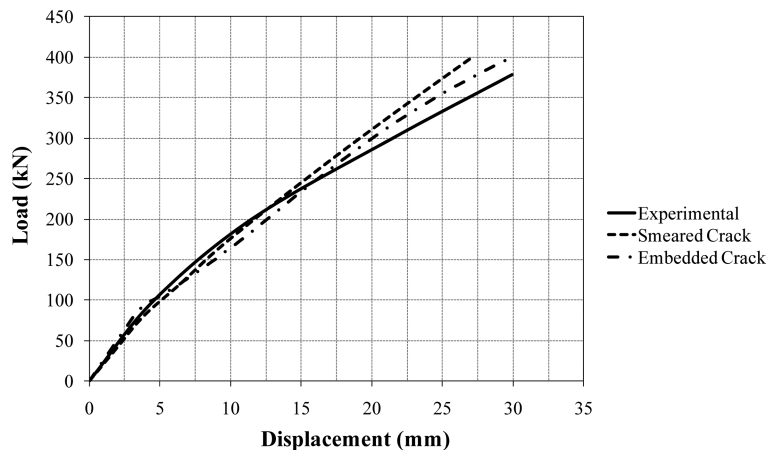


Fig. 7 Load-displacement curves obtained for the OA3 beam tested by Bresler and Scordelis (1963)

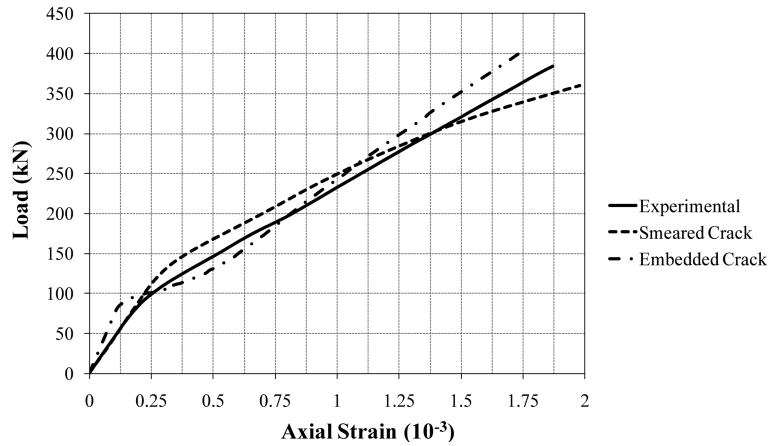


Fig. 8 Load-strain curves of bottom reinforcement steel obtained for OA3 beam tested by Bresler and Scordelis (1963)

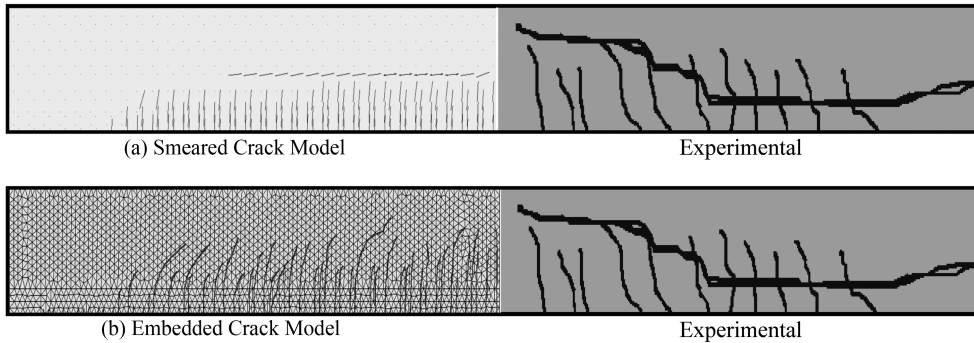


Fig. 9 Crack patterns obtained for the OA3 beam tested by Bresler and Scordelis (1963)

tension reinforcement bars, in the mid-span position (Fig. 8).

The resulting responses show a good correlation between the results of the implemented crack models and the experimental responses. A stiffer behavior was observed in the tension rebars at loads below the cracking load using the embedded crack approach. This behavior is probably due to the fact that the nodal displacement components associated to the discontinuity are subtracted from the displacement vector (Eq. (2)). This problem can be solved by reducing Young's modulus in the rebars or even by using interface elements coupled to adherence constitutive models.

With respect to the crack patterns obtained (Fig. 9), both models exhibit a slight slope of the larger cracks, tending to form the rupture shear band shown in the experimental crack pattern. The embedded crack model produces crack spacing closer to the experimental pattern. The numerically determined shear crack trajectory of the beam shown in Fig. 9 matches reasonably well the trajectories observed in the test, despite the difficulties in capturing such a phenomenon in a numerical simulation.

Fig. 10 presents results in terms of crack openings. The maximum opening observed in the tests was 0.35 mm, while the numerical simulation with the smeared crack and the embedded crack models resulted, respectively, in 0.40 mm and 0.48 mm. This indicates that the smeared crack

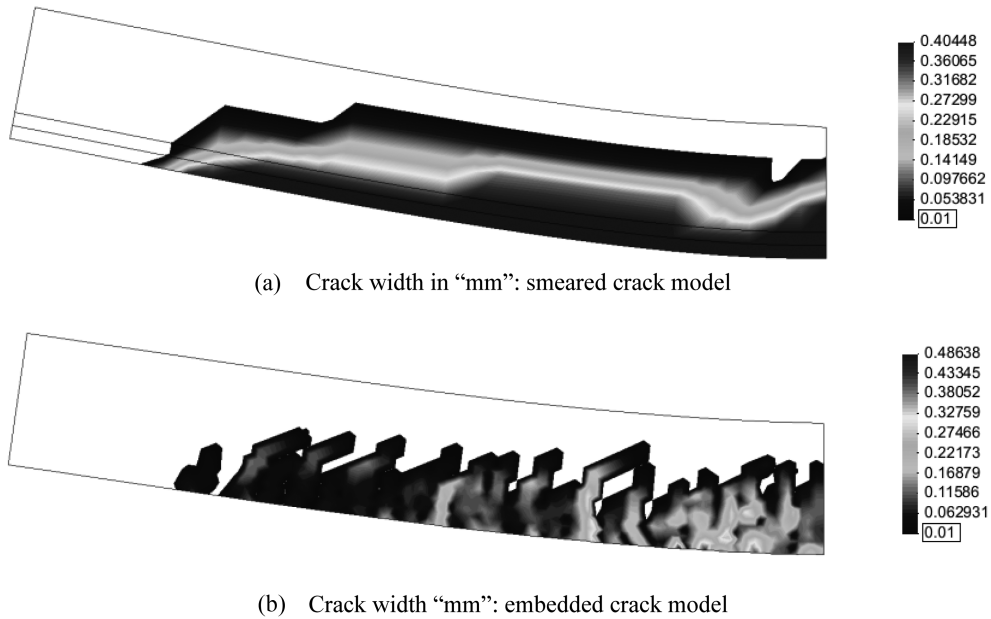


Fig. 10 Crack width obtained for the OA3 beam tested by Bresler and Scordelis (1963)

models, though simple in comparison to other models (discrete or embedded crack approaches) and presenting mesh dependence, are capable of predicting the behavior of reinforced concrete structures with reasonable accuracy.

The smeared crack models lose accuracy mainly at high values of crack opening, i.e. larger discontinuities (above 1.0 mm). In this case, the embedded crack approach is more interesting and useful.

#### 4.2 Vecchio's beam

The B3 beam, which was first tested in Berkeley (Bresler and Scordelis 1963) and later in Toronto (Vecchio and Shim 2004), was modeled with the two different strategies described above. Fig. 11 illustrates details of test setup and beam geometry.

Fig. 12 through Fig. 14 illustrate the force-displacement curves, crack openings and crack patterns for the Toronto B3 beam.

A good correlation between numerical and experimental results can be observed from the force-

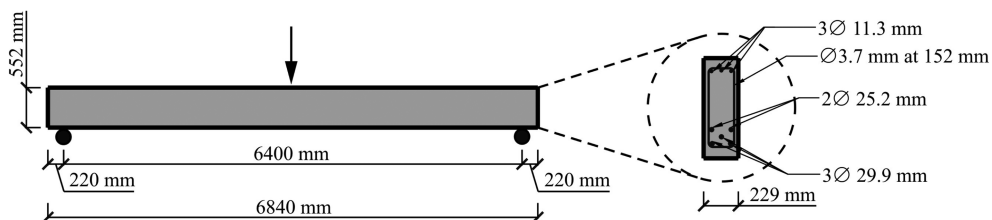


Fig. 11 Test setup for the B3 beam tested in Toronto (Vecchio and Shim 2004)

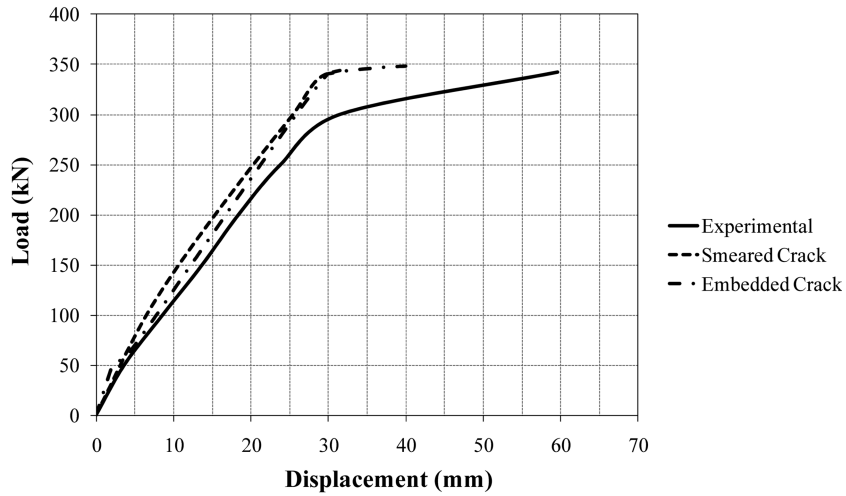


Fig. 12 Load-displacement curves obtained for the B3 beam tested by Vecchio and Shim (2004)

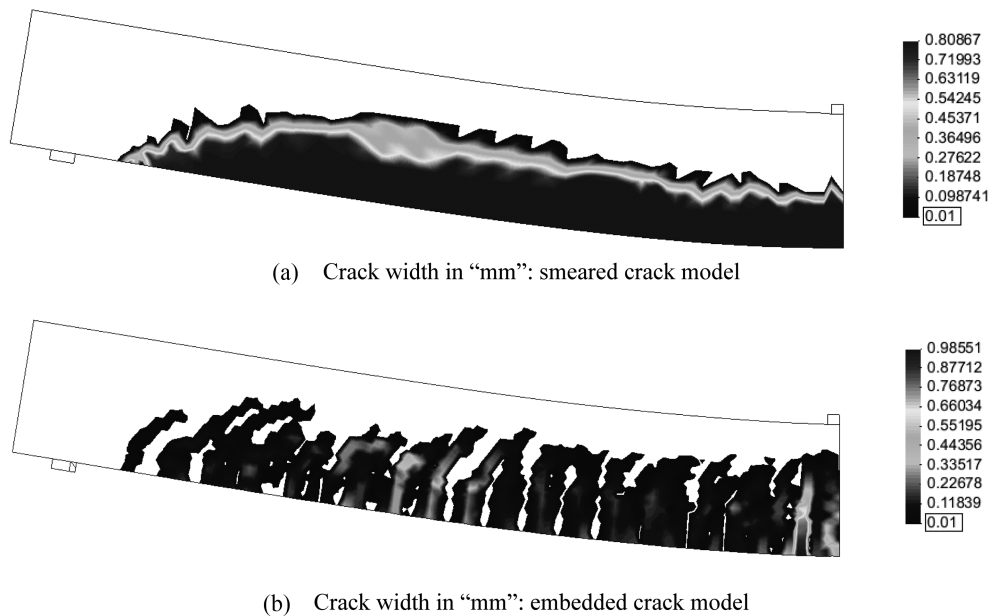


Fig. 13 Crack width obtained for the B3 beams tested by Vecchio and Shim (2004)

displacement curves. With respect to the crack openings, the maximum value observed was 1.60 mm, while the smeared crack and embedded crack models resulted, respectively, in 0.80 mm and 0.98 mm. The crack patterns predicted by the embedded crack approach match the observed pattern better than that predicted by the smeared crack model, mainly insofar as crack spacing and extension is concerned.

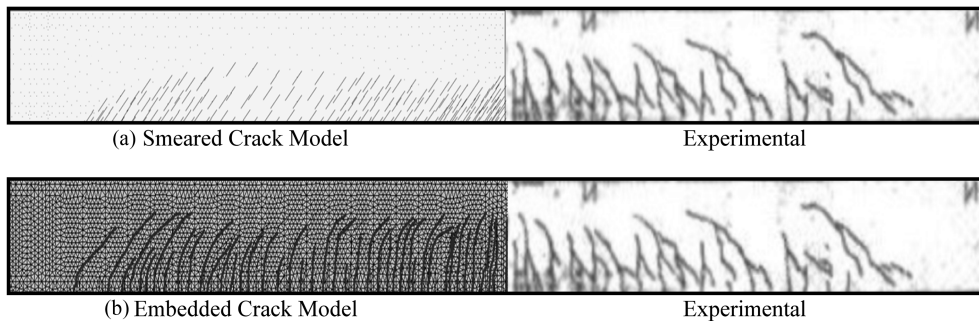


Fig. 14 Crack patterns obtained for the B3 beam tested by Vecchio and Shim (2004)

## 5. Conclusions

The determination of crack openings in two-dimensional modeling of reinforced concrete structures via the Finite Element Method, using a rotational smeared crack model and an embedded crack model, was addressed here. The following conclusions can be drawn from these numerical simulations:

- The crack patterns numerically obtained for the beam tested in Berkeley (Bresler and Scordelis 1963) presented a slight slope of the larger cracks, thus tending towards a shear rupture band, as indicated in the experimental pattern. The embedded crack model produced a crack spacing more compatible with the experimental observation. The maximum crack openings were 0.35 mm, 0.40 mm and 0.48 mm, respectively, for the experimental observation, smeared crack model and embedded crack model.
- For the Toronto beam (Vecchio and Shim 2004), the maximum crack openings were 1.60 mm, 0.80 mm and 0.98 mm, respectively, for the experimental observation, smeared crack model and embedded crack model.
- The embedded crack model presented here is based on the enrichment of the three-node finite element, which is thus able to properly describe the effects of a single crack crossing its interior. The application of this model to the analysis of reinforced concrete members, in which the nonlinear behavior is strongly influenced by the formation of several cracks with small spacing, requires the use of fine meshes to describe the crack pattern. The smeared model can deal with this situation using coarser meshes, with the expense of using higher-order elements.
- In general, the embedded crack model presented more realistic results with respect to crack trajectories as well as crack openings. Although this model requires finer meshes to capture multiple cracks, low-order finite elements (a three-node element in this case) can be used.

These findings indicate some tendencies in the characteristics of the two distinct approaches chosen for the present comparative study.

## Acknowledgements

The authors wish to express their gratitude and appreciation to FAPESP–State of São Paulo Research Foundation (Grants 06/05843-2 and 04/03049-1) and to CNPq–National Council for

Scientific and Technological Development (Grants 304915/2005-0, 307051/2006-4 and 306678/2006-3) for their financial support of this research.

## References

- Bresler, B. and Scordelis, A.C. (1963), "Shear strength of reinforced concrete beams", *J. Am. Concrete Inst.*, **60**(1), 51-74.
- Cervera, M., Oliver, J. and Manzoli, O.L. (1996), "A rate-dependent isotropic damage model for the seismic analysis of concrete dams", *Earthq. Eng. Struct. D.*, **25**(9), 987-1010.
- Gamino, A.L., Bittencourt, T.N. and Sousa, J.L.A.O. (2009), "Finite element computational modeling of externally bonded CFRP composites flexural behavior in RC beams", *Comput. Concrete*, **6**(3), 187-202.
- Gamino, A.L., Bittencourt, T.N. and Sousa, J.L.A.O. (2007), "Numerical modeling of classic concrete beam tests", *IBRACON Struct. J.*, **3**(2), 201-229. (Available from [http://www.ibracon.org.br/publicacoes/revistas\\_ibracon/rev\\_estruturas/](http://www.ibracon.org.br/publicacoes/revistas_ibracon/rev_estruturas/))
- Gamino, A.L. (2007), *Physical and computational modeling of RC structures strengthened with FRP*, PhD Thesis, Escola Politécnica, Universidade de São Paulo, São Paulo. (in Portuguese)
- Gamino, A.L. and Bittencourt, T.N. (2007), "Numerical evaluation of plastic rotation capacity in reinforced-concrete beams", *6<sup>th</sup> International Conference on Fracture Mechanics of Concrete and Concrete Structures - FraMCoS 6*, Catania, **2**, 665-670.
- Jacomassi, L.M.C., Gamino, A.L. and Barbosa, M.P. (2009), "Numerical simulation of the behavior of reinforced concrete beams by FEM using CASTEM 2000 Program", *Rev. Int. Mét. Num. Cál. Dis. Ing.*, **25**(2), 133-144.
- Jirásek, M. and Zimmermann, T. (1998), "Analysis of rotating crack model", *J. Eng. Mech. - ASCE*, **124**(8), 842-851.
- Jirásek, M. (2000), "Comparative study on finite elements with embedded cracks", *Comput. Method. Appl. M.*, **188**, 307-330.
- Lorrain, M.S., Barbosa, M.P., Arnaud, M. and Gamino, A.L. (2007), "High strength concrete: the reinforced concrete of the century 21<sup>st</sup>?", *Rev. Int. Mét. Num. Cál. Dis. Ing.*, **23**(3), 251-264.
- Manzoli, O.L., Oliver, J., Huespe, A.E. and Diaz, G. (2008), "A mixture theory based method for three dimensional modeling of reinforced concrete members with embedded crack finite elements", *Comput. Concrete*, **5**(4), 401-416.
- Manzoli, O.L. and Shing, P.B. (2006), "A general technique to embed non-uniform discontinuities into standard solid finite elements", *Comput. Struct.*, **84**(10-11), 742-757.
- Ngo, D. and Scordelis, A.C. (1967), "Finite element analysis of reinforced concrete beams", *ACI J.*, **64**(3), 152-163.
- Oliver, J., Linero, D., Huespe, A. and Manzoli, O.L. (2008), "Two dimensional modeling of material failure in reinforced concrete by means of a continuum strong discontinuity approach". *Comput. Method. Appl. M.*, **197**, 332-348.
- Oliver, J., Cervera, M. and Manzoli, O. (1999), "Strong discontinuities and continuum plasticity models: the strong discontinuity approach", *Int. J. Plasticity*, **15**, 319-351.
- Oliver, J. (2000), "On the discrete constitutive models induced by strong discontinuity kinematics and continuum constitutive equations", *Int. J. Solids Struct.*, **37**, 7207-7229.
- Ottosen, N.S. (1977), "A failure criterion for concrete", *J. Eng. Mech. Division*, **103**(4), 527-535.
- Vecchio, F.J. and Shim, W. (2004), "Experimental and analytical re-examination of classic concrete beam tests", *J. Struct. Eng. - ASCE*, **130**(3), 460-469.